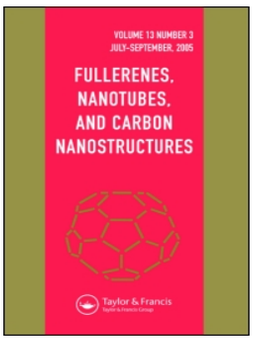

Fullerenes, Nanotubes and Carbon Nanostructures

ISSN: 1536-383X (Print) 1536-4046 (Online) Journal homepage: http://www.tandfonline.com/loi/lfnn20

Copper complexes within the supramolecular solid structure of cyanuric acid and melamine

Roberto C. Dante, Francisco M. Sánchez-Árevalo, Pedro Chamorro-Posada, José Vázquez-Cabo, Luis Lartundo-Rojas, Jaime Santoyo-Salazar, Rubén Mendoza-Cruz, J. Jesús Velázquez-salazar, M. Josefina Arellano-Jiménez, J. Enrique Samaniego & Omar Solorza-Feria

To cite this article: Roberto C. Dante, Francisco M. Sánchez-Árevalo, Pedro Chamorro-Posada, José Vázquez-Cabo, Luis Lartundo-Rojas, Jaime Santoyo-Salazar, Rubén Mendoza-Cruz, J. Jesús Velázquez-salazar, M. Josefina Arellano-Jiménez, J. Enrique Samaniego & Omar Solorza-Feria (2016) Copper complexes within the supramolecular solid structure of cyanuric acid and melamine, Fullerenes, Nanotubes and Carbon Nanostructures, 24:11, 688-697, DOI: 10.1080/1536383X.2016.1223633

To link to this article: http://dx.doi.org/10.1080/1536383X.2016.1223633

Accepted author version posted online: 19 Aug 2016.
Published online: 19 Aug 2016.

FULLERENES, NANOTUBES AND CARBON NANOSTRUCTURES
2016, VOL. 24, NO. 11, 688–697
http://dx.doi.org/10.1080/1536383X.2016.1223633

Taylor & Francis
Taylor & Francis Group

Copper complexes within the supramolecular solid structure of cyanuric acid and melamine

Roberto C. Dante[a], Francisco M. Sánchez-Árevalo[b], Pedro Chamorro-Posada[c], José Vázquez-Cabo[d], Luis Lartundo-Rojas[e], Jaime Santoyo-Salazar[f], Rubén Mendoza-Cruz[g], J. Jesús Velázquez-salazar[g], M. Josefina Arellano-Jiménez[g], J. Enrique Samaniego[h], and Omar Solorza-Feria[i]

[a]R&D Department, 2D to 3D S.r.l.s. Via Santuario 27/B, Moretta (CN), Italy; [b]Instituto de Investigaciones en Materiales, Universidad Nacional Autónoma de México, Apdo. Postal 70-360, Cd. Universitaria, México D.F., Mexico; [c]Dpto. de Teoría de la Señal y Comunicaciones e IT, Universidad de Valladolid, ETSI Telecomunicación, Paseo Belén 15, Valladolid, Spain; [d]Dpto. de Teoría de la Señal y Comunicaciones, Universidad de Vigo, ETSI Telecomunicación, Lagoas Marcosende s/n, Vigo, Spain; [e]Instituto Politécnico Nacional, Centro de Nanociencias y Micro y Nanotecnologías de Nanociencias, UPALM, Zacatenco México-D.F., México; [f]Departamento de Física, Centro de Investigación y de Estudios Avanzados del Instituto Politécnico Nacional (CINVESTAV-IPN). Apdo. Postal 14-740, México D.F., México; [g]Department of Physics & Astronomy, University of Texas at San Antonio, One UTSA Circle, San Antonio, Texas, USA; [h]Centro de Investigación y de Estudios Avanzadosdel Instituto Politécnico Nacional (CINVESTAV-IPN). Libramiento Norponiente 2000, Real de Juriquilla, Queretaro, C.P, Mexico; [i]Departamento de Química, Centro de Investigación y de Estudios Avanzados del Instituto Politécnico Nacional (CINVESTAV-IPN). Av. IPN 2508, Col. San Pedro Zacatenco, Apdo. Postal 14-740 , México D.F., Mexico

ABSTRACT

A complex of copper sulfate was formed by impregnation of the cyanuric acid melamine adduct (CAM) with a solution of copper (II) sulfate. A thermal treatment at 250°C of the dried compound delivered a greenish powder. The UV-Vis spectroscopy showed that an absorption around 700 nm is compatible with a copper (II) sulfate complex coordinated inside the supramolecular structure of CAM. No copper or copper oxide particles were found by means of either transmission or scanning electron microscopy. X-ray photoelectron spectroscopy showed that on the surface there was a considerable amount of Cu(I) (66%) probably coordinated also inside the CAM channels. A brief catalytic test showed the ability of the copper complexes to oxidize sucrose to gluconic acid.

ARTICLE HISTORY
Received 20 June 2016
Accepted 9 August 2016

KEYWORDS
Melamine cyanurate; Copper complexes; THz spectroscopy; Supramolecular solids

Introduction

The research presented in this report on cyanuric acid and melamine adducts started from the synthesis of polymeric carbon nitride, which is a very popular carbon material for its versatility and the many potential applications (1–15). However, the precursor, i.e. the cyanuric acid and melamine adduct (CAM), used in our synthesis, exhibited interesting characteristics by itself since it is a supramolecular solid, hold only by hydrogen bonds, with the ability to host molecules in channels and cavities behaving as a solid solvent. In Figure 1, the rosette-shaped cavity of diameter of approximately 4 Å—large enough to host small molecules and transition metal ions—is shown (16).

In brief, this research started in a reverse way: we realized that the precursor may exhibit interesting properties. The CAM precursor treated with sulfuric acid at different temperatures was studied in a previous report to follow its transformation to polymeric carbon nitride. Actually, we noticed that sulfuric acid could interact with CAM retarding its decomposition as a solute does, so that we found interesting to introduce as a probe a coordination complex to follow investigating the interaction of a ionic complex with the 3D structure of CAM. Copper sulfate was introduced into CAM to better investigate this supramolecular solid and to discover the possibilities that it offered as both a hosting material and a solid solvent. Moreover, copper sulfate IR and UV-vis spectral characteristics are well known and can vary depending on coordination providing us information about the environment in which is embedded. The idea of using melamine and cyanuric acid compounds as the basis to design self-assembling started with Zerkowski et al. (17), they denominated the most plausible structures as tape and rosette types. Ranganathan et al. (16) confirmed that the CAM adducts are of the rare cases of organic solids which contain channels. It is noteworthy to point out that Choi et al. prepared rod shaped particles self-assembled from the lattice of CAM compounds such as (18). Recently, attention was focused on self-assembled monolayers (SAM) based on either melamine or cyanuric acid (19–21). For example, a molecular network of melamine with featured pores of subnanometer size was prepared on the Au(111) surface, and was found to be able to trap gold adatoms and concomitant single vacancies (21).

Either catalytic or sensor properties can also be searched in the 3D networks of CAM with the formation of metal complex that can be hosted inside the material cages and channels. In this study, X-ray diffractometry (XRD), Fourier

CONTACT Roberto C. Dante rcdante@yahoo.com R & D Department, 2D to 3D S.r.l.s. Via Santuario 27/B, 12033, Moretta CN, Italy.
Color versions of one or more of the figures in the article can be found online at www.tandfonline.com/lfnn.

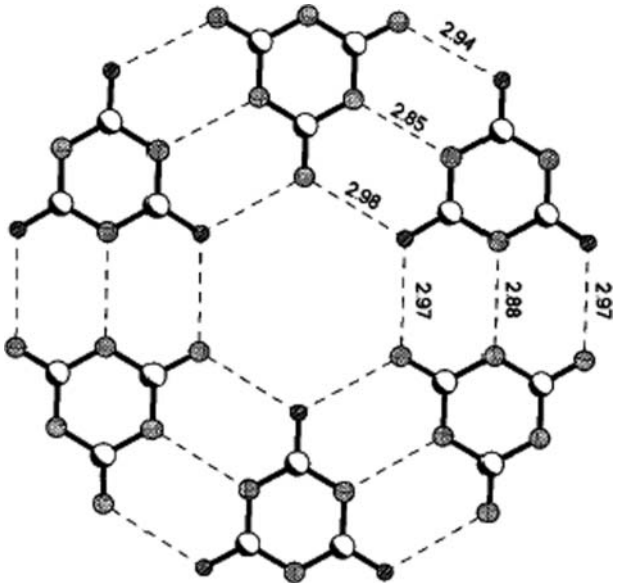

Figure 1. Rosette cage of the cyanuric acid and melamine adduct able to host molecules and metal ions (16).

transform infrared spectroscopy (FTIR), UV-visible spectroscopy, as well as the innovative Tera-Hertz time domain spectroscopy (THz-TDS) were used to determine the effect of the presence of copper in the CAM framework, vibrational lattice modes related to the stacked sheet structure. The material was also characterized by scanning (SEM) and transmission electron microscopy (TEM). X-ray photoelctron spectroscopy (XPS) allowed us to identify the types of copper sites and their interaction.

The ability of the Cu complex embedded in CAM to act as a catalyst towards glucose oxidation by hydrogen peroxide was briefly tested. The main product of glucose oxidation detected by IR spectroscopy was gluconic acid.

Materials, experimental, and theoretical methods

Materials

Melamine cyanurate was supplied by Nachmann S.r.l.s.u. (Italy) with a purity higher than 99%. Melamine cyanurate was treated with 0.1M Cu(II) sulfate solution overnight, filtered and dried at 110°C for 6 hours to favor dispersion of copper within melamine cyanurate. The sulfate treated sample of about 4 g, was subsequently placed in microwave oven and treated at 250°C for 30 min.

Structural characterization

FT-IR spectroscopy

The infrared spectra were obtained by means of a Agilent Carey 630 transform-infrarred (FT-IR) sepectrometer (Agilent, USA). The IR spectra were obtained directly from solutions and solids by attenuated total reflectance (ATR). A brief qualitative reaction of sucrose oxidation in ethanol at 70°C was performed in order to check the catalytic activity of the CAM Cu complex.

X-ray diffraction measurements

The X-ray diffraction patterns were obtained by means of a powder diffractometer Rigaku ULTIMA-IV with Cu Kα radiation. Glass capillaries for sample mounting were used. The samples were ground in an agate mortar and sifted. The measurements always lasted for 1 hour, and crystalline silicon was used as a standard.

TEM and SEM characterization

In addition, the CAM Cu complex was studied by transmission electron microscopy (TEM) with a JEM-FS2010 HRP (JEOL, Japan). A scanning electron microscope (SEM) Hitachi SEM 1510 (Hitachi, Japan) was used to observe the particles morphology at lower magnifications. In addition, the scanning transmission electron microscope (STEM) JEM-ARM200F (JEOL, Japan) was used to study the morphology and composition of the samples by the energy dispersion spectroscopy.

Thermal analysis

The thermal stability and decompostion rate of supamolecular intermediates in of polymeric carbon nitride from melamine cyanurate was evaluated by thermogravimetric analysis using a STD Q600 thermobalace (TA Instruments, USA) with an nitrogen mass flow rate of 25 mL/min and a temperature raye of 10°C/min.

UV-Vis spectroscopy

UV-Vis diffuse reflectance spectra were measured using a Perkin Elmer Lambda 35 UV-Vis spectrophotometer. A Spectralon® blank was used as reference. The reflectance data were transformed to absorbance data applying the Kubelka–Munk method as follows:

$$F(R) = \frac{(1-R)^2}{2R} \quad (1)$$

Where R is the reflectance and $F(R)$ is the Kubelka–Munk (K–M) function. The K–M function was plotted as a function of the energy ($E = hc/\lambda$) and the band gap value was calculated through the inflection point of this curve. The abscissa of this point is directly associated with the band-gap value (22).

Tera Hertz-time domain spectroscopy measurements

A Menlo Tera K15 Spectrometer was used for the THz-TDS analysis. The system is based on a 1560 nm fiber laser that generates 90 fs pulses at a repetition rate of 100 MHz. This provides a compact fiber-coupled setup. The system was operated in a nitrogen rich atmosphere in order to avoid the signature of water absorption in the recorded samples. Ten sample and ten references measurements were performed in each case in order to reduce the noise in the measurements.

The material parameters in the spectral range of interest were calculated from the time domain photocurrent traces measured with the spectrometer. These time domain waveforms depend not only on the material data but also on the width of the pellets due to the contributions from multiple reflections at the pellet-air interfaces. Signal processing techniques similar to those described by Duvillaret et al. (23) were employed in order to obtain the THz spectra of the materials.

X-ray photoelectron spectroscopy

The chemical composition of the two samples was examined ex situ by XPS surface measurements. The C1s, O1s, N1s, S2p, Cu2p, and survey spectra were recorded using a Thermo Scientific K-Alpha instrument. Monochromatic X-ray source Al Kα (1486.6 eV) was used for all samples and experiments. The X-Ray monochromatic spot was 400 μm in diameter. Residual vacuum in the analysis chamber was maintained at around 6•10^{-9} mbar. The binding energies (BEs) positions were referenced to the C1s on unsputtered surfaces. Charge referencing was done by setting the binding energy of C 1s photo peak at 285 eV C1s adventitious carbon contribution. We have also employed an electron flood gun to minimize surface charging (Charge compensation). Correct charge compensation is demonstrated in all samples by overlapping the C1s signal before and after experiment. The atomic concentrations were determined from the XPS peak areas using the Shirley background subtraction technique and the Scofield sensitivity factors. Some fragments of the samples were fixed to the sample holder with a double side copper adhesive tape.

Quantum chemistry computations

The semiempirical quantum chemistry computations were performed with the PM6 method (24) using the parallel implementation for multi-threaded shared-memory CPUs and massively parallel GPU acceleration (25) of the MOPAC2012 (26) software package. A Fedora Linux server with a 12 cores Intel Xeon processor and a NVIDIA Tesla K20 GPU was used for the computations.

In the Supplementary Section, more details on the following photocatalysis tests, procedure, and results were provided.

Results and discussion

Structural characterization

Infrared spectroscopy

The IR spectrum of CAM (see Figure 2) is dominated by the absorptions due to three chemical groups: NH_2, OH, and carbonyl CO, in addition, to other modes, associated specifically to the triazine ring. Both melamine and cyanuric acid belong to the D3h point group, their vibrational modes were already studied and assigned to the modes of this group (27,28). However, the symmetry of each type of triazine is distorted by the H-bonds and many absorptions which are usually not active become active in IR too. The peaks at 3377 and 3227 cm^{-1} (both *E'* modes) correspond to the asymmetric and symmetric NH_2 stretching absorptions, respectively. The broad band around 2500 cm^{-1} may correspond to amide NH interacting via hydrogen bonding with oxygen within cyanuric acid. The peaks at 1778 and 1731 cm^{-1} are attributed to the carbonyl stretching of cyanuric acid. The peak at 1655 cm^{-1} corresponds to the NH_2 bending (including amide of the cyanuric acid), *A'* mode, while the peak at 1531 cm^{-1} is attributed to a C-N asymmetric stretching in the ring (*E'*). The peak at 1447 cm^{-1} can be attributed mainly to a side-chain C-N breathing (A_1'). The peak at 1200 cm^{-1} may be an overtone of NH_2 wagging. Both peaks at 1084 cm^{-1} s and 1031 cm^{-1} correspond to ring breathing (A_1"). The peak at 764 cm^{-1} belongs to a side-chain CN vibration (A_2"), and 810 cm^{-1} belongs to a ring out of plane deformation mode (*E'*).

The spectra of the pure CAM, that of the CAM Cu (1CAM Cu) nonthermally treated, and that of the CAM Cu (2 CAM Cu) treated at 200°C are shown in Figure 1. The spectra of CAM as is and that of CAM Cu not thermally treated do not show any specific difference, indicating that copper sulfate did not interact with CAM, but that thermally treated exhibited a considerable shoulder at 1330 cm^{-1} due to the coordination of copper in the CAM framework. This band can be due to a mode of cyanuric acid in the lactim form, the OH bending is made more active possibly for the decreasing of the H-bonding with melamine, which in turn is involved in coordinating copper ions.

X-ray diffraction pattern

The XRD pattern of 2 CAM Cu is shown in Figure 3 and is substantially compatible with that of pure CAM. However, the 2CAM Cu sample exhibited more ancillary peaks around the main peak assigned to the 002 reflection ($d = 3.21$ Å) than the pure CAM in the region between 18 and 40°, highlighted by the box in Figure 2.

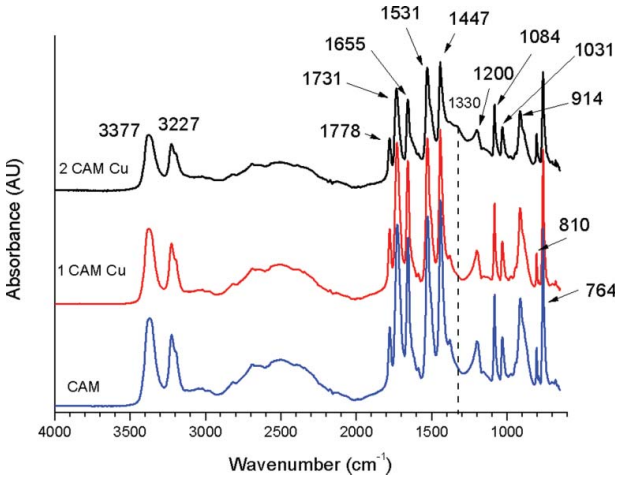

Figure 2. IR spectra: complex of cyanuric acid and melamine as is (CAM), nonthermally treated complex of copper sulfate and CAM (1 CAM Cu), CAM Cu treated at 200°C (2CAM Cu).

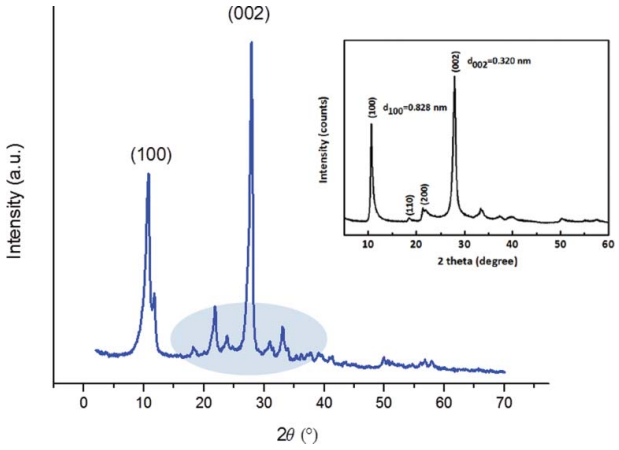

Figure 3. XRD pattern of 2 CAM Cu (CAM Cu treated at 200°C). In the inset, the XRD pattern of pure CAM (29).

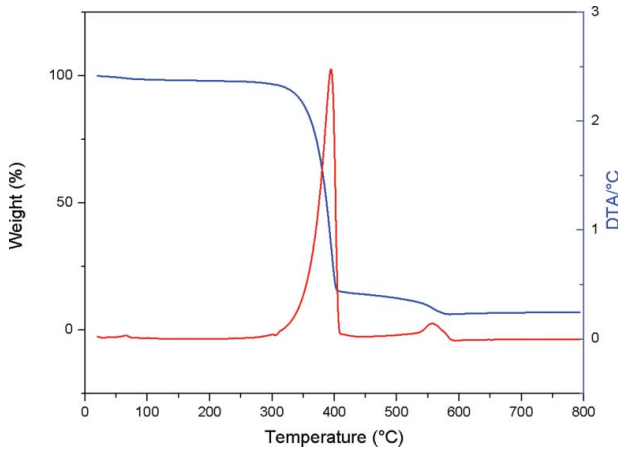

Figure 4. Thermal gravimetric analysis of CAM Cu sample.

There is another ancillary peak at 11.8° ($d = 7.71$ Å) close to the 001 reflection at 10.7° ($d = 8.29$ Å). These ancillary peaks can be due to distortions and modulations (including density modulations) (30) caused by the presence of copper coordinated inside the lattice, which alter the supramolecular H-bonded frame.

Thermal gravimetric analysis (TGA)

The thermal gravimetric analysis curve and the differential thermal analysis (DTA) signal are shown in Figure 4. The massive weight loss at 400°C corresponds to the CAM decomposition, the second loss to the decomposition of the polymeric carbon nitride (31), which was formed in completion with decomposition in gaseous compounds. The residue above 600°C is around the 6.5 wt % corresponding to the amount of copper sulfate trapped by CAM.

Morphology of the CAM Cu: SEM and TEM analysis

A small amount of CAM Cu (few miligrams) was suspended in ethanol, sonicated and a fraction of the suspended material was observed at both SEM and TEM. No particles of copper oxides were observed by both SEM and TEM analysis. Moreover, the distribution of Cu and S seemed to be quite uniform on the surface as shown by the EDS mapping obtained with the STEM Arm200F (see Figure 5).

For sake of brevity, only two images obtained by the JEM-FS2010 are shown. The lamellar structure of the material can be better seen on the edges where the stacked layers tend to be unfolded (see Figure 6). It is noteworthy to point out that most suspended particles seem to be composed of few layers of the CAM complex.

UV-Vis spectroscopy

UV-Vis diffuse reflectance spectrum of 2 CAM Cu is presented in Figure 7. This shows two bands: one around 200 nm and the other around 700 nm. These bands should not be confused with those of polymeric carbon nitride (31) since in CAM Cu these are due to the copper complexes. More recently, Cu(II) sulfate was used as to obtain Cu-doped polymeric carbon nitride from melamine cyanurate(32). Our results shows that using a Cu(II) sulfate solution, and a slight temperature treatment (heating the sample at 250°C for 30 minutes) an electronic transition at energies lower than polymeric carbon nitride appeared due to the copper complexes (32,29). The two main absorptions at 200 and 700 nm caused the greenish color of the product.

The curve deconvolution showed that the real maximum of the band around 700 nm is 760 nm, which correspond to a hydrated Cu(II) sulfate according to (33). The temperature treatment of 250°C probably induced a reaccomodation of the copper (II) sulfate complex, where water molecules (after treatment at this temperature Cu(II) sulfate is dehydrated (34)) were substituted, for example, by the OH of cyanuric acid inside the rosette cages of CAM, causing a color variation as found also in some Cu(II) nanofluids(35). This is compatible with the IR changes caused by the presence of copper sulfate, especially the appearance of the shoulder at 1330 cm^{-1} associated to a complex with melamine and cyanuric acid (36). It noteworthy to highlight

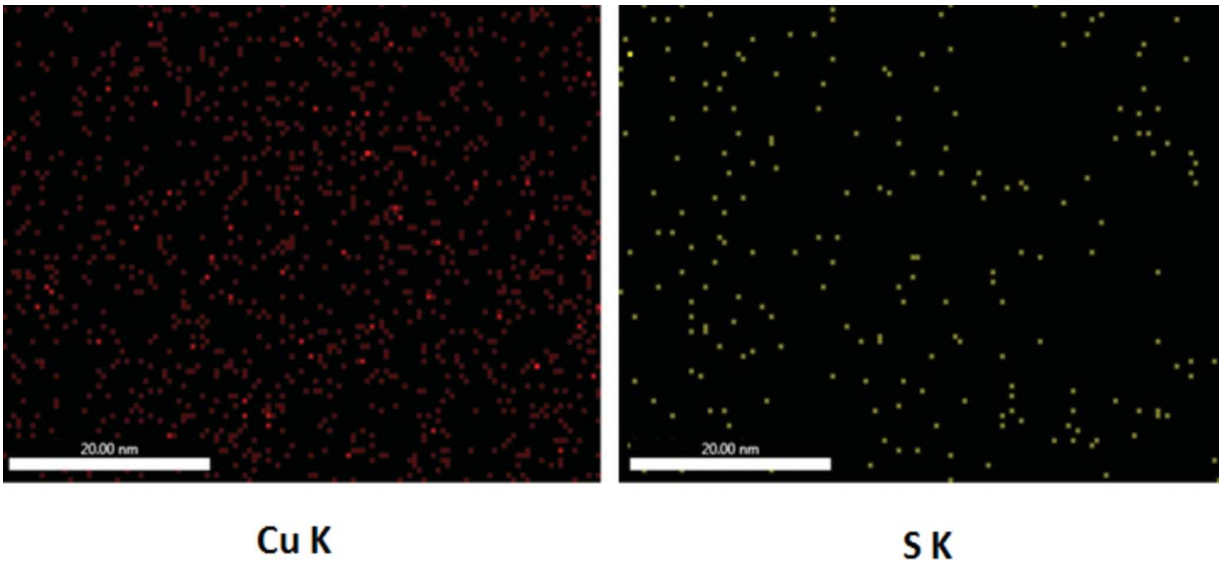

Figure 5. Cu and S mapping of the surface of a CAM Cu particle obtained by EDS of the STEM ARM 200 F.

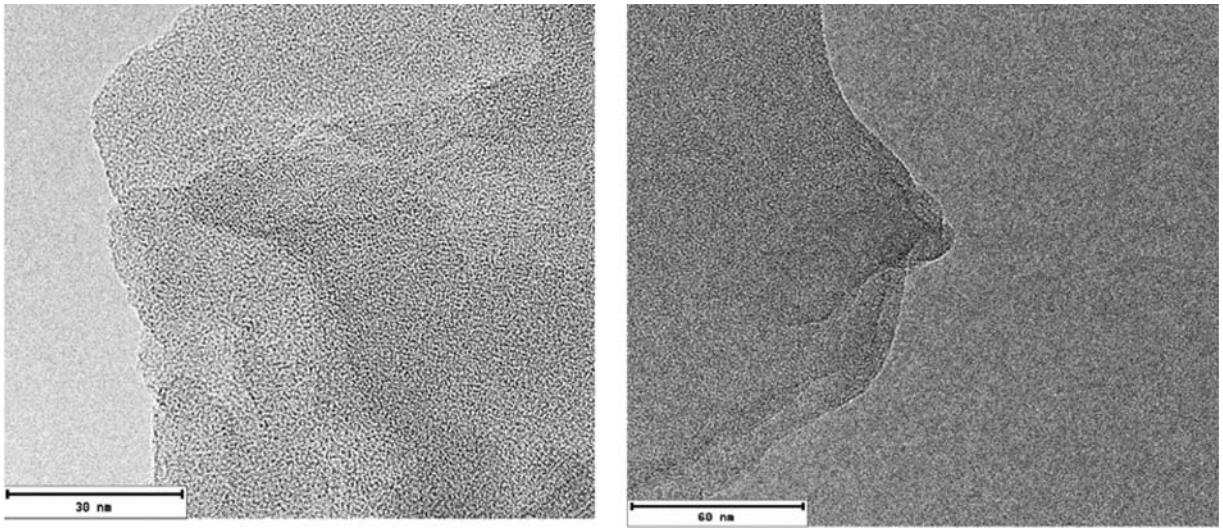

Figure 6. TEM images of the CAM Cu suspended particles showing the detail of the layers exposed on the particle edges.

that also our complexes are in a certain way solvated as nanofluids. However, copper (I) oxide or sulfate does not exhibit absorptions in the Uv-vis range.

The possible coordination product is shown in Figure 8, showing either Cu (II) or Cu(I) coordinated in the cages of CAM by cyanuric acid, melamine and sulfate ion.

X-ray photoelectron spectroscopy

The XPS survey scan of the CAM sample showed the presence of C1s, N1s, O1s, as depicted in Figure 9 corresponding to the composition of cyanuric acid melamine adduct.

To compensate surface-charging effects, the binding energy (BE) of the core level C(1s) was set at 285 eV(33).

XPS peaks deconvolution allowed to extract the different peaks components being then possible a chemical state interpretation.

Moreover, we performed the deconvolution of the C1s spectra referencing the main peak at 285 eV(37), which is assigned both to carbon atoms bounded to Carbon atoms and hydrogen atoms. The spectra and peak deconvolutions of C1s and N1s were displayed in Figure 10.

The BEs of C1s high-resolution spectrum (CAM sample) were identified as follows; C1 (284.9 eV), C2 (286.3 eV), C3 (288.3 eV), and C4 (290.0 eV) were attributed to C-CH_2, C-O and C-N, C=O, carboxyl, C=O, respectively. While C5 (295.8 eV) corresponds to the Skape up satellite due the transition $\pi \rightarrow \pi^*$ of delocalized electrons (33).

The contributions of nitrogen into the CAM structure also were characterized by peak fitting in N1s region. The peaks can be identified as N1 (399.1 eV), N2 (400.6 eV), which are attributed to the amino group NH_2, pyrrolic nitrogen C-N-C, respectively. Moreover, N3 (406.2 eV) is associated to $\pi \rightarrow \pi^*$ transition shake-up satellites. The O1s peak was characterized by an intense peak at 532.29 eV which essentially corresponds to the carbonyl oxygen of cyanuric acid, and for sake of brevity it is not reported. A satellite peak was localized at 539.95 eV.

In Figure 11, the C1s, N1s, Cu2p, and S2p of CAM Cu core-level photoemission spectra are shown. It is possible to see that the peaks of C1s, N1s are substantially inaltered indicating that also the CAM structure did not undergo any change due to the copper presence. The O1s peak, not displayed for sake of brevity, was also inaltered. Although, the Cu2p peaks were weak, it was possible to distinguish between Cu(I) and Cu(II) species. Their peaks position of $Cu2p_{3/2}$ were situated at 932.64, and 934.93 eV, attributed to Cu(I) and Cu(II), respectively (39). The corresponding peaks of $Cu2p_{1/2}$ were found at 952.5 eV and 955.0 eV for Cu(I) and Cu(II), respectively. The copper shake-up peaks are located around 945 and 942 eV for Cu(I) and Cu(II), respectively. It was determined that Cu(I) is the 66% of total so that most surface copper (II) was reduced to Cu(I).

Moreover, S2p peaks essentially corresponded to sulfur of the sulfate ion SO_4^{2-} (41).

The quantitative elemental analysis is resumed in Table 1 for both CAM and CAM Cu samples. The composition corresponded in both cases to that of the cyanuric acid and melamine complex with C/N ratio close to 1 since both

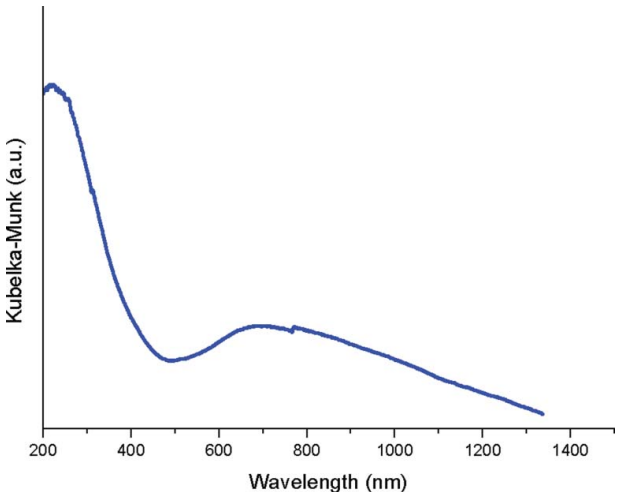

Figure 7. UV-Vis diffuse reflectance (Kubelka–Munk) spectra for the CAM Cu sample.

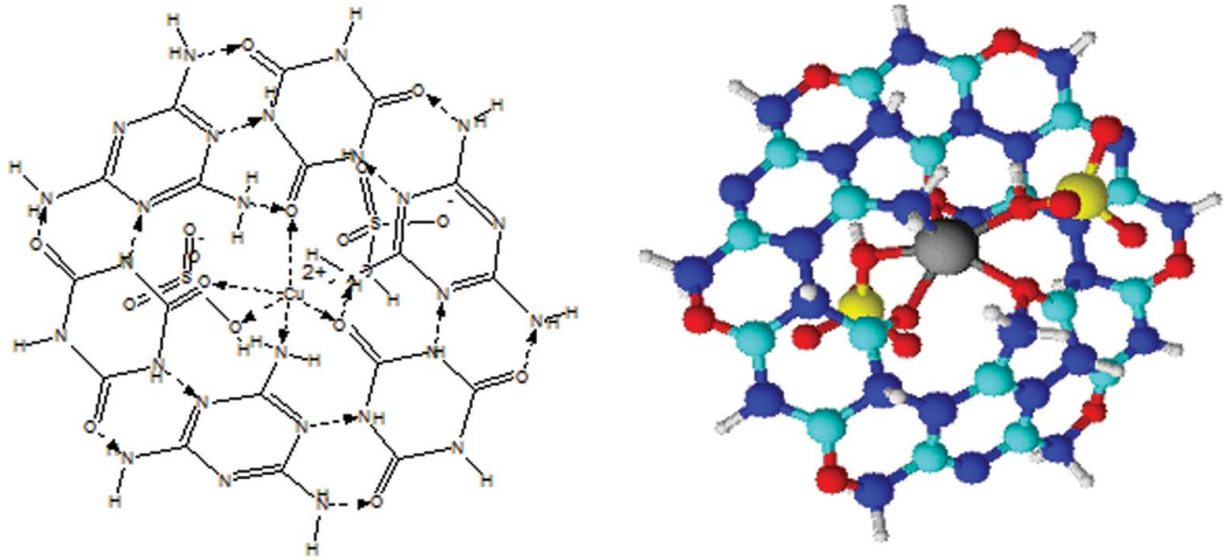

Figure 8. Cu^{2+} coordination in the CAM rosette channel, a similar situation may occur for Cu^{+}.

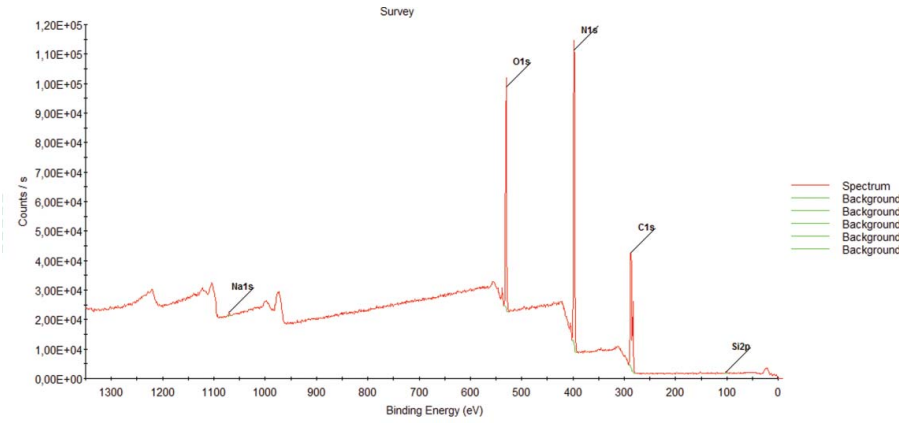

Figure 9. XPS Survey of CAM alone showing the presence of C1s, N1S, and O1s as well as that of some impurities.

cyanuric acid and melamine has a C/N ratio of 1. Moreover, the Cu/S ratio indicates that a part of Cu is not yet bonded to sulfur at least on the surface. Possibly, Cu(I) is probably formed by the oxidation of melamine to melaminium and hosted and coordinated in the CAM cages, since copper oxide particles were not detected by SEM or TEM analysis.

Semi-empirical quantum chemistry calculations

The experimental crystal structure of the CAM adduct determined in (16) was used as initial guess in the numerical calculations. The reported CAM crystal is monoclinic with lattice parameters a = 14.853 Å, b = 9.641 Å, c = 3.581 Å β= 92.26°. In the CAM crystal, the relative positions of the N and C ring atoms of the CA and M units are identical (16) and the relative

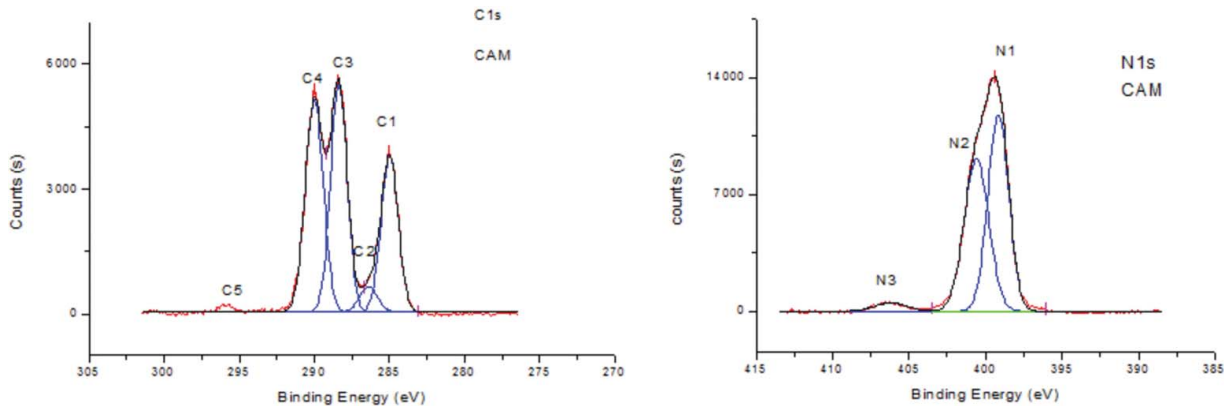

Figure 10. XPS spectrum of C1s and N1s of CAM sample with deconvolution peaks.

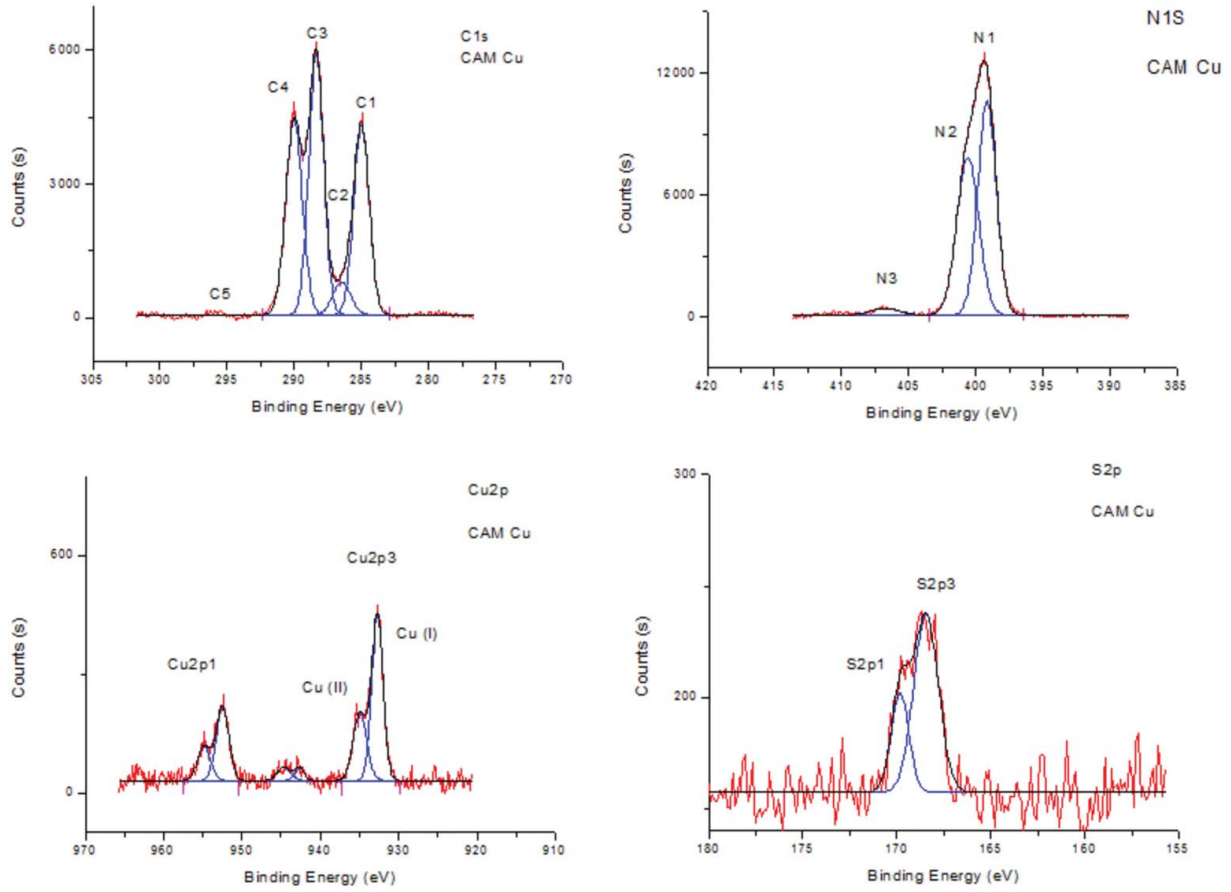

Figure 11. C1s, N1s, Cu2p, S2p XPS spectra and deconvolution peaks of CAM Cu.

positions of the O atoms in CA are very close to those of the N of the amine groups in M. Therefore, interchanging the CA and M positions in alternate layers does not have any relevant impact on the predicted XR diffraction pattern.

Calculations performed using MOPAC with the PM3, PM6, and PM7 Hamiltonians failed to converge when the initial crystal structure as given in (16) was used. Nevertheless, convergence to an accurate geometry could be obtained when the CA and M positions in adjacent MAC layers were interchanged. Among the NNDO semi-empirical methods, PM6 typically provides a very good compromise between accuracy and the tight convergence level required for the calculation of the lattice vibrations (39). The geometry optimized using the PM6 method has unit cell parameters a = 14.882 Å, b = 9.920 Å, c = 7.364 Å, $\alpha = 90.55°$, $\beta = 94.03°$ and $\gamma = 90.29°$ in very good agreement with the experimental data, after doubling the spatial period along the c axis.

Accuracy restrains in solid state calculations using MOPAC set a minimum size for the computational unit cell (40). This often requires to increase the computational domain to include several crystal unit cell. In our case, we had to extend the computation cell to 1×1×2 unit cells so a sphere with a diameter of at least 8 Å can be fitted in it. The vibrations calculated in this manner include modes that do not satisfy the k≈0 condition, which is a requirement, arising from momentum conservation considerations, for a relevant contribution to the vibrational spectra (39). Therefore, the calculated frequencies have to be processed in order to select those for which the crystal unit cells comprising the computational domain oscillate approximately in phase and, therefore, match the k≈0 condition, to predict the absorption spectra of materials (39).

For the optimized geometry, two of the computed modes with a relevant transition dipole satisfy the aforementioned condition in the terahertz band, with respective frequencies of 1.22 THz and 2.15 THz and transition dipoles of 0.154 D and 0.209 D, respectively. The calculated modes are displayed in Figures 12 (a) and (b). The resonance at 1.22 THz is associated with in-plane displacements distorting the rosette structure. The resonance at 2.15 THz corresponds to a lattice mode involving the rocking of several rings in the MCA adduct. Moreover, since the oscillations are in phase for all the layers in the computational unit cell, it is expected that these modes should also provide a good description of the vibration spectrum in an arrangement without the alternation of layers, with the interchange of the M and CA units as well.

THz-TDS measurements

The materials were pressed under identical conditions (7 tm and 5 min) to form pellets of small width w ≤400 μm in order

Table 1. Atomic percent of the both CAM and CAM Cu samples as determined by XPS.

atomic %	C	O	N	C/N ratio	Cu/S
CAM	40.99	16.37	41.98	0.98	—
CAM Cu	43.17	14.88	40.79	1.05	1.27

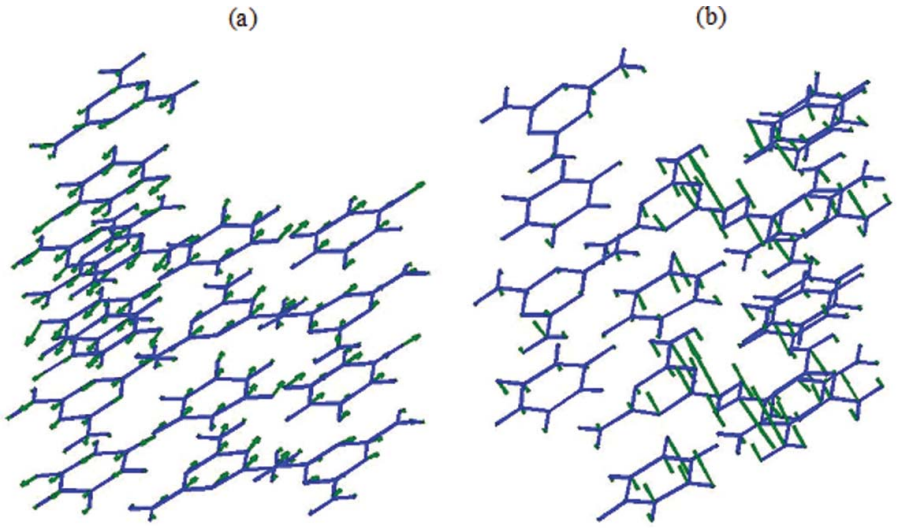

Figure 12. Two views of the domain used in the semi-empirical quantum chemistry calculations and the atomic displacements corresponding to the two vibration modes at 1.22 THz (a) and 2.15 THz (b).

to limit the total propagation loss low and maximize the dynamic range.

The measured THz spectra are shown in Figure 13. Instead of defined resonances, they display the broadened attenuated feature typical of disordered materials (41,42) in the THz band, with a monotonic increase from the low frequency edge. Above 2 THz, the measurement is limited by the available dynamic range. Even though the global shapes of the spectra of the two materials are very similar, there is a noticeable reduction in the attenuation of the Cu doped sample, which can be attributed to the incorporation of some Cu in the CAM adduct channel. Even though measurements have been performed in a nitrogen rich atmosphere, the faint spectral features at 1.7 THz correspond to water vapor absorption lines are due to the presence of residual humidity (43).

Results of photocatalytic oxidation

Catalytic activity of the CAM Cu complex was briefly tested and compared with a blank without CAM Cu. A 10 ml solution of sucrose in ethanol at 10 wt % was treated with 10 ml of hydrogen peroxide at 5 wt% in the presence of CAM Cu (10 mg) and another aliquot without the potential catalyst. Each sample was treated for 27 min at 80°C. The IR spectra of the samples with and without CAM Cu, as well as that of sucrose in water are displayed in Figure 14.

The region between 1200 and 800 cm^{-1} is characterized by a combination of modes of C-O and C-C vibrations of C-OH groups. The spectrum of sucrose treated for 27 min at 80°C is similar to that of glucose with a shoulder on the water OH bending peak, around 1700 cm^{-1}, corresponding to carbonyl stretching of the aldehyde of glucose.

Moreover, the spectrum of the specimen treated in the presence of CAM Cu showed a stronger band of carbonyl around 1700 cm^{-1} overlaid to that of OH bending of water and two remarkable peaks at 1402 and 1272 cm^{-1} corresponding, respectively, to C-O-H bending and C-O stretching of carboxylic acids.

The broad band of OH stretching also showed a different structure from the other spectra attributable to the OHs of carboxylic acid.

In summary, the reaction catalyzed by CAM Cu led to the oxidation of glucose to the carboxylic acid named gluconic acid

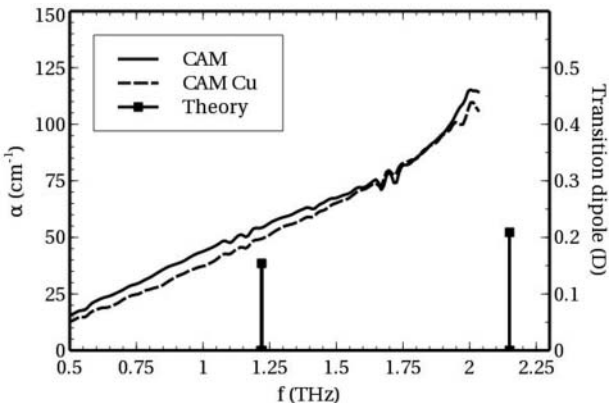

Figure 13. Measured THz spectra for CAM and Cu CAM and the theoretically calculated vibration modes.

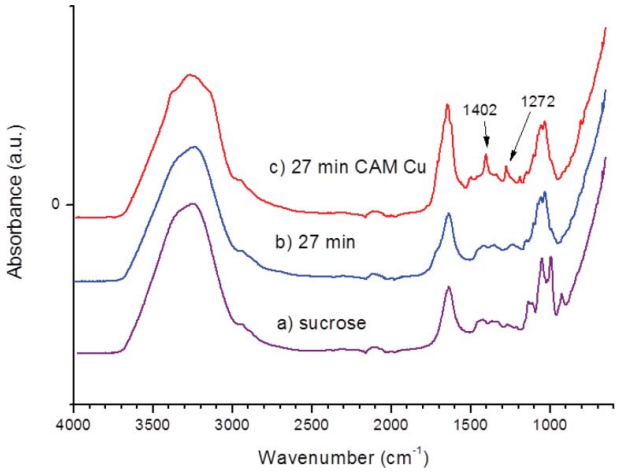

Figure 14. IR spectra of (a) sucrose in water, (b) after 27 min of treatment with H_2O_2 at 80°C, (c) after 27 min of treatment with H_2O_2 at 80°C in the presence of CAM Cu.

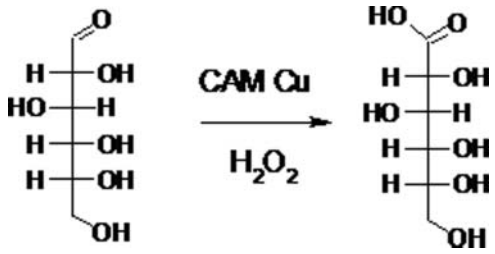

Figure 15. Oxidation of glucose to gluconic acid catalyzed by CAM Cu.

(see Figure 15), which is a powerful chelant of several metallic cations (44). The ability of copper (I, II) complexes to specifically catalyze the oxidation of aldhydes to carboxylic acids was already reported by us in a previous report on polymeric carbon nitride complex of copper (32).

Conclusions

A complex of copper sulfate was formed by impregnation of the cyanuric acid melamine adduct (CAM) with a solution of copper (II) sulfate. A thermal treatment at 250°C of the dried compound delivered a greenish powder. The UV-Vis spectroscopy showed that an absorption around 700 nm is compatible with a copper (II) sulfate complex coordinated inside the supramolecular rosette structure of CAM. No copper or copper oxide particles were found by means of both TEM and SEM. XPS and XRD results showed that the cyanuric acid-melamine framework was only slightly altered by the presence of copper. Moreover, a considerable amount of Cu(I) (66%) was found on the surface by XPS, which was probably coordinated also inside the CAM cavities as Cu(II). The THz spectrum showed a continuous attenuation increment with frequency, compatible with the behavior of a disordered material. However, attenuation decreased at low frequencies (~1THz), possibly due to the hindrance caused by copper coordination. A brief catalytic test showed the ability of the copper complexes to oxidize sucrose to gluconic acid using hydrogen peroxide.

References

1. Cohen, M.L. (1985) Calculation of bulk moduli of diamond and zinc-blende solids. *Phys Rev B Condens Matter.*, 32: 7988–7991.
2. Liu, A.Y., and Cohen, M.L. (1990) Structural properties and electronic structure of low-compressibility materials: beta-Si_3N_4 and hypothetical beta-C_3N_4. *Phys. Rev. B Condens. Matter.*, 41: 10727–10734.
3. Li, X., Zhang, J., Shen, L., Ma, Y., Lei, W., Cui, Q., and Zou, G. (2008) Preparation and characterization of graphitic carbon nitride through pyrolysis of melamine. *Appl. Phys. A.*, 94: 387–392.
4. Zhao, Y., Liu, Z., Chu, W., Song, L., Zhang, Z., Yu, D., Tian, Y., Xie, S., and Sun, L. (2008) Large-scale synthesis of nitrogen-rich carbon nitride microfibers by using graphitic carbon nitride as precursor. *Adv. Mater.*, 20: 1777–1781.
5. Dante, R.C., Martín-Gil, J., Pallavidino, L., and Geobaldo, F. (2010) Synthesis under pressure of potential precursors of CNx materials based on melamine and phenolic resins. *J. Macromol. Sci. B.*, 49: 371–382.
6. Zhang, G., Zhang, M., Ye, X., Qiu, X., Lin, S., and Wang, X. (2014) Iodine modified carbon nitride semiconductors as visible light photocatalysts for hydrogen evolution. *Adv. Mater.*, 26: 805–809.
7. Zhang, J., Sun, J., Maeda, K., Domen, K., Liu, P., Antonietti, M., Fu, X., and Wang, X. (2011) Sulfur-mediated synthesis of carbon nitride: band-gap engineering and improved functions for photocatalysis. *Energy Environ. Sci.*, 4: 675–678.
8. Zhang, Y., Bo, X., Nsabimana, A., Luhana, C., Wang, G., Wang, H., Li, M., and Guo, L. (2014) Fabrication of 2D ordered mesoporous carbon nitride and its use as electrochemical sensing platform for H_2O_2, nitrobenzene, and NADH detection. *Biosens. Bioelectron.*, 53: 250–256.
9. Zhang, Y., Mori, T., and Ye, J. (2012) Polymeric carbon nitrides: Semiconducting properties and emerging applications in photocatalysis and photoelectrochemical energy conversion. *Sci. Adv. Mater.*, 4: 282–291.
10. Zhang, Y., Schnepp, Z., Cao, J., Ouyang, S., Li, Y., Ye, J., and Liu, S. (2013) Biopolymer-activated graphitic carbon nitride towards a sustainable photocathode material. *Scientific Rep.*, 3: 2163.
11. Vinu, A., Ariga, K., Mori, T., Nakanishi, T., Hishita, S., Golberg, D., and Bando, Y. (2005) Preparation and characterization of well-ordered hexagonal mesoporous carbon nitride. *Adv. Mater.*, 17: 1648–1652.
12. Zhao, H., Lei, M., Yang, X., Jian, J., and Chen, X. (2005) Route to GaN and VN Assisted by carbothermal reduction process. *J. Am. Chem. Soc.*, 127: 15722–15723.
13. Zimmerman, J.L., Williams, R., Khabashesku, V.N., and Margrave, J.L. (2001) Synthesis of spherical carbon nitride nanostructures. *Nano Lett.*, 1: 731–734.
14. Cao, C., Huang, F., Cao, C., Li, J., and Zhu, H. (2004) Synthesis of carbon nitride nanotubes via a Catalytic-assembly solvothermal route. *Chem. Mater.*, 16: 5213–5215.
15. Thomas, A., Fischer, A., Goettmann, F., Antonietti, M., Müller, J.-O., Schlögl, R., and Carlsson, J.M. (2008) Graphitic carbon nitride materials: variation of structure and morphology and their use as metal-free catalysts. *J. Mater. Chem.*, 18: 4893–4908.
16. Ranganathan, A., Pedireddi, V. R., and Rao, C.N.R. (1999) Hydrothermal synthesis of organic channel structures: 1:1 Hydrogen-bonded adducts of melamine with cyanuric and trithiocyanuric acids. *J. Am. Chem. Soc.*, 121: 1752–1753.
17. Zerkowski, J.A., Seto, C.T., and Whitesides, G.M. (1992) Solid-state structures of rosette and crinkled tape motifs derived from the cyanuric acid melamine lattice. *J. Am. Chem. Soc.*, 114: 5473–5475.
18. Choi, I.S., Li, X., Simanek, E.E., Akaba, R., and Whitesides, G.M. (1999) Self-assembly of hydrogen-bonded polymeric rods based on the cyanuric acid • melamine lattice. *Chem. Mater.*, 11: 684–690.
19. Papageorgiou, A.C., Fischer, S., Reichert, J., Diller, K., Blobner, F., Klappenberger, F., Allegretti, F., Seitsonen, A.P., and Barth, J.V. (2012) Chemical transformations drive complex Self-assembly of uracil on close-packed coinage metal surfaces. *ACS Nano*, 3: 2477–2486.
20. Silly, F., Shaw, A.Q., Castell, M.R., Briggs, G.A.D., Mura, M., Martsinovich, N., and Kantorovich, L. (2008) Melamine structures on the Au(111) surface. *J. Phys. Chem. C*, 112: 11476–11480.
21. Wang, L., Chen, Q., Shi, H., Liu, H., Ren, X., Wang, B., Wu, K., and Shao, X. (2016) Metal adatoms generated by the co-play of melamine assembly and subsequent CO adsorption. *Phys. Chem. Chem. Phys.*, 18: 2324–2329.
22. Nowak, M., Kauch, B. and Szperlich, P. (2009) Determination of energy band gap of nanocrystalline SbSI using diffuse reflectance spectroscopy. *Rev. Sci. Instrum.*, 80: 046107.
23. Duvillaret, L., Garet, F., and Coutaz, J.L. (1996) A reliable method for extraction of material parameters in terahertz time-domain spectroscopy. *IEEE J. Sel. Top. Quant.*, 2: 739–746.
24. Stewart, J.J.P. (2007) Optimization of parameters for semiempirical methods V: Modification of NDDO approximations and application to 70 elements. *J. Mol. Model.*, 13: 1173–1213.
25. Maia, J.D.C., Carvalho, G.A.U., Mangueira, C.P., Santana, S.R., Cabral, L.A.F., and Rocha, G.B. (2012) GPU linear algebra libraries and GPGPU programming for accelerating MOPAC semiempirical quantum chemistry calculations. *J. Chem. Theory Comput.*, 8: 3072–3081.
26. Stewart, J.J.P. (2012) *Stewart Computational Chemistry*, Colorado Springs, CO, USA, Available at http://openmopac.net
27. Gunasekaran, S., Srinivasan, K., and Raja, S.X.J. (1993) Fourier transform infrared and laser Raman scattering studies on the structure of melamine. *Proc. Indian natn. Sci. Acad.*, 59A: 347–352.

28. Mircescu, N.E., Oltean, M., Chis, V., and Leopold, N. (2012) FTIR, FT-Raman, SERS and DFT study on melamine. *Vib. Spectrosc.*, 62: 165–171.
29. Jun, Y., Lee, E.Z., Wang, X., Hong, W.H., Stucky, G.D., and Thomas, A. (2013) From melamine−cyanuric acid supramolecular aggregates to carbon nitride hollow spheres. *Adv. Funct. Mater.*, 23: 3661–3667.
30. Janssen, T., and Janner, A. (2014) Aperiodic crystals and superspace concepts. *Acta Cryst*., B70: 617–651.
31. Dante, R.C., Martín-Ramos, P., Sánchez-Arévalo, F.M., Huerta, L., Bizarro, M., Navas-Gracia, L.M., and Martín-Gil, J. (2013) Synthesis of crumpled nanosheets of polymeric carbon nitride from melamine cyanurate. *J. Solid State Chem.*, 201: 153–163.
32. Dante, R.C., Sánchez-Arévalo, F.M., Chamorro-Posada, P., Vázquez-Cabo, J., Huerta, L., Lartundo-Rojas, L., Santoyo-Salazar, J., Solorza-Feria, O., Diaz-Barrios, A., Zoltan, T., Vargas, F., Valenzuela, T., Muñoz-Bisesti, F., and Quiroz-Chávez, F.J. (2016) Synthesis and characterization of Cu-doped polymeric carbon nitride. *Fuller. Nanotubes. Carbon Nanostruct.*, 24: 171–180.
33. Swadzba-Kwasny, M., Chancelier, L., Ng, S., Manyar, H. G., Hardacre, C., and Nockemann, P. (2012) Facile in situ synthesis of nanofluids based on ionic liquids and copper oxide clusters and nanoparticles. *Dalton Trans.*, 41: 219–227.
34. Shirasuka, K., Shimizu, S., and Sugimaru, N. (1995) Thermal decomposition of crystalline pentahydrous copper (II) sulfate. *Inorg. Mater.*, 2: 127–128.
35. Haber, V. (1977) Study of the amorphous product of dehydration of copper(II) sulfate pentahydrate. *Chem. Zvesti*, 31: 190–196.
36. Wiles, A.B., Bozzuto, D., Cahill, C.L., and Pike, R. D. (2006) Copper (I) and (II) complexes of melamine. *Polyhedron*, 25: 776–782.
37. Briggs, D., and Seah, M.P. (1990) *Practical Surface Analysis Volume 1: Auger and X-ray Photoelectron Spectroscopy*, 2nd ed., J Wiley: London.
38. Vasquez, R. P. (1998) $CuSO_4$ by XPS. *Surf. Sci. Spectra*, 5: 279–284.
39. Chamorro-Posada, P. (2008) Study of the terahertz spectra of crystalline materials using NDDO semi-empirical methods: polyethylene, poly(vinylidene fluoride) form II and α-D-glucose. *arXiv:1604.03919*.
40. Stewart, J.P.P. (2008) Application of the PM6 method to modeling the solid state. *J. Mol. Model.*, 14: 499–535.
41. Walther, M., Fisher, B.M., and Jepsen, P.U. (2003) Noncovalent intermolecular forces in polycrystalline and amorphous saccharides in the far infrared. *Chem. Phys.*, 288: 261–268.
42. Chamorro-Posada, P., Vázquez-Cabo, J., Rubiños-López, O., Martín-Gil, J., Hernández-Navarro, S., Martín-Ramos, P., Sánchez-Arévalo, F. M., Tamashausky, A.V., Merino-Sánchez, C., and Dante, R.C. (2016) THz TDS study of several sp^2 carbon materials: Graphite, needle coke and graphene oxides. *Carbon*, 98: 484–490.
43. Rothman, L.S., Gordon, I.E., Babikov, Y., Barbe, A., Benner, D.C., Bernath, P.F., Birk, M., Bizzocchi, L., Boudon, V., Brown, L.R., Campargue, A., Chance, K., Cohen, E.A., Coudert, L.H., Devi, V.M., Drouin, B.J., Fayt, A., FlaudJ.-M., Gamache, R.R., Harrison, J.J., Hartmann, J.-M., Hill, C., Hodges, J.T., Jacquemart, D., Jolly, A., Lamouroux, J., Le Roy, R.J., Li, G., Long, D.A., Lyulin, O.M., Mackie, C.J., Massie, S.T., Mikhailenko, S., Müller, H.S.P., Naumenko, O.V., Nikitin, A.V., Orphal, J., Perevalov, V., Perrin, A., Polovtseva, E.R., Richard, C., Smith, M.A.H., Starikova, E., Sungi, K., Tashkun, S., Tennyson, J., Toon, G.C., Tyuterev, Vl. G., and Wagner, G.J. (2012) The HITRAN2012 molecular spectroscopic database. *J. Quant. Spectrosc. Radiat. Transfer*, 130: 4–50.
44. Nikolić, V.D., Ilić, D. P., Nikolić, L.B., Stanojević, L.P., Cakić, M.D., Tačić, A.D., and Ilić-Stojanović, S. S. (2014) The synthesis and characterization of iron (II): Gluconate. *Adv. Technol.*, 3: 16–24.